Raman scattering in C_{60} and $C_{48}N_{12}$ aza-fullerene: First-principles study

Rui-Hua Xie* and Garnett W. Bryant

National Institute of Standards and Technology, Gaithersburg, Maryland 20899-8423

Vedene H. Smith, Jr.

Department of Chemistry, Queen's University, Kingston, Canada ON K7L 3N6

(Received 26 July 2002; revised manuscript received 2 December 2002; published 11 April 2003)

We carry out large-scale *ab initio* calculations of Raman scattering activities and Raman-active frequencies (RAF's) in $C_{48}N_{12}$ aza-fullerene. The results are compared with those of C_{60}. Twenty-nine nondegenerate polarized and 29 doubly degenerate unpolarized RAF's are predicted for $C_{48}N_{12}$. The RAF of the strongest Raman signal in the low- and high-frequency regions and the lowest and highest RAF's for $C_{48}N_{12}$ are almost the same as those of C_{60}. The study of C_{60} reveals the importance of electron correlations and the choice of basis sets in the *ab initio* calculations. Our best calculated results for C_{60} with the B3LYP hybrid density functional theory are in excellent agreement with experiment and demonstrate the desirable efficiency and accuracy of this theory for obtaining quantitative information on the vibrational properties of these molecules.

I. INTRODUCTION

In 1985, C_{60}, a fascinating molecule formed as a truncated icosahedron with 20 hexagonal and 12 pentagonal faces and 60 vertices, was discovered by Kroto *et al.*[1] Since then, a third form of pure carbon, called *fullerenes*,[2] has been extensively studied. This kind of molecule can crystallize in a variety of three-dimensional structures,[3,4] with an even number of three-coordinated sp^2 carbon atoms that arrange themselves into 12 pentagonal faces and any number (>1) of hexagonal faces.[2] The macroscopic synthesis of soot,[3] which contains C_{60} and other fullerenes in large compounds, plus the straightforward purification techniques, which make pure fullerene materials available, opened new research opportunities in science, engineering, and technology.[5–9] In the meantime, doped fullerenes have also attracted a great deal of researchers' interest due to their remarkable structural, electronic, optical, and magnetic properties.[5–9] For example, doped tubular fullerenes can exhibit large third-order optical nonlinearities[8] and be ideal candidates as photonic devices[7] for all-optical switching, data processing, and eye and sensor protection (optical limiter). Another example is alkali-metal-doped C_{60} crystals, which can be superconducting.[5] Because of their unique structure and electronic properties,[5] fullerenes can be doped in several different ways including endohedral doping,[5,10] substitutional doping,[11–16] and exohedral doping.[5–7,9]

Since the average carbon-carbon bond length in C_{60} is slightly larger than that in graphite, which can only be doped by boron, and the force constants[5] are somewhat weakened by the curvature of the C_{60} surface, both boron and nitrogen can substitute for one or more carbon atoms in C_{60}.[11–16] In 1991, Guo, Jin, and Smalley[11] successfully synthesized boron-substituted fullerenes $C_{60-n}B_n$ with n between 1 and at least 6. In 1995, Hummelen *et al.*[12] reported a very efficient method of synthesizing $C_{59}N$, which has led to a number of detailed studies of the physical and chemical properties of $C_{59}N$.[6,7,9,13] Recently, Hultman *et al.*[14] have synthesized nitrogen-substituted derivatives of C_{60} with more

than one nitrogen atom and reported the existence of a novel $C_{48}N_{12}$ aza-fullerene.[14,15] Very recently, we have studied the bonding, electronic structure, Mulliken charge, infrared (IR) spectrum, and NMR of $C_{48}N_{12}$ by using density functional theory (DFT) and the 6-31G basis set.[16] We characterized 58 IR spectral lines and eight ^{13}C and two ^{15}N NMR spectral signals of $C_{48}N_{12}$ and demonstrated that this aza-fullerene has potential applications as semiconductor components for nanometer electronics because of its small energy gap, as a promising electron donor for molecular electronics, and as a good diamagnetic material because of the enhancement of diamagnetic factors in the carbon atoms.[16] The characterization of $C_{48}N_{12}$ is a timely problem both from the viewpoint of its practical applications and to understand doping in C_{60} derivatives. In the present paper, we characterize the Raman spectrum of $C_{48}N_{12}$.

As a material is doped with foreign atoms, its mechanical, electronic, magnetic, and optical properties change.[5,7] The ability to control such induced changes is vital to progress in material science. Raman and IR spectroscopic techniques[17,18] are basic, useful experimental tools to investigate how doping modifies the structural and dynamical properties of the pristine material and to understand the physical origin of such induced changes. Over the past 10 years, both techniques have been widely used to study the vibrational properties of C_{60},[19–24] its derivative compounds,[25,26] and (doped) carbon nanotubes.[27] It has been shown that C_{60} has in total 46 vibrational modes including 4 IR-active[19–22] and 10 Raman-active[23,24] vibrational modes. Well-resolved Raman spectra[25] are also available for C_{60} and a number of its derivative compounds.

In this paper, we perform first-principles calculations of Raman scattering activities (RSA's) and Raman-active frequencies (RAF's) in both $C_{48}N_{12}$ and C_{60} using DFT and the restricted Hartree-Fock (RHF) method. Very recently, Choi *et al.*[28] have theoretically assigned all 46 vibrational modes of C_{60}, including a scaling of the force field by using Pulay's method. In this paper, however, we carry out *ab initio* a series of calculations for C_{60}. We want to test the efficiency

and accuracy of such first-principles calculations and study, in detail, basis set effects on RSA's and RAF's by comparing our theoretical results with available experiments.[5,23–26] To the best of our knowledge, such basis set effects on the RSA's and RAF's of C_{60} have not been considered before. These calculations for C_{60} give us a benchmark for assigning the Raman-active vibrational modes of $C_{48}N_{12}$ and provide us with constructive insight into the microscopic mechanisms responsible for the difference between $C_{48}N_{12}$ and C_{60}. We find that the 10 RAF's for C_{60}, obtained by using a hybrid DFT method and large basis sets, are in excellent agreement with Raman experiments. We predict that $C_{48}N_{12}$ aza-fullerene has 58 RAF's including 29 nondegenerate polarized modes and 29 doubly degenerate unpolarized modes.

This paper is organized as follows. Section II briefly reviews the *ab initio* methods, basis sets, and the theory of calculating Raman scattering activities. Section III presents our Raman results for both C_{60} and $C_{48}N_{12}$ obtained by using RHF and DFT methods, and the results are compared to results obtained by other theoretical methods. Our conclusions are given in Sec. IV.

II. THEORY

A. *Ab Initio* methods and basis sets

Ab initio methods obtain information by solving variationally the Schrödinger equation without fitting parameters to experimental data. Instead, experimental data guide the selection of the *ab initio* methods rather than directly entering the computational procedures. Fullerenes have been challenging molecules for *ab initio* calculations because of their size.[29] Recent advances in *ab initio* electronic structure methods and parallel computing have brought a substantial improvement in the capabilities to predict and study the properties of large molecules. The coupled cluster method[30] has been used to predict phenomena in C_{20}.[31] Other *ab initio* methods, which are less demanding in terms of computation cost than the coupled cluster method, have been used for much larger fullerenes and carbon nanotubes, for example, C_{60} (Refs. 32 and 33 with self-consistent field and Moller-Plesset second-order (MP2) theory, C_{240} (Ref. 34) and carbon nanotubes (Ref. 35) with DFT, and C_{540} (Ref. 36) with the HF method. The major expense in HF and DFT calculations arises from solving the electronic quantum Coulomb problem. The effective Hamiltonian diagonalization (a procedure that scales as N_b^3, N_b being the number of basis functions) represents only a minor portion of the computational time in calculations of molecular clusters containing up to several hundred atoms.[37] In addition, DFT (Ref. 38) requires an additional three-dimensional numerical quadrature to obtain the exchange and correlation energies.[30] Both HF and DFT methods have been implemented into the GAUSSIAN 98 program.[39] In this paper, all calculations are performed by using the GAUSSIAN 98 program.[39,40]

One of the approaches inherent in all *ab initio* methods is the introduction of a basis set.[30] If the basis set is complete, exact expansions of the molecular orbitals can be obtained. However, a complete basis set requires an infinite number of functions, which is impossible in actual calculations. Gener-

ally, a smaller basis set provides a poorer representation. Moreover, only the parts of the molecular orbital which correspond to the selected basis can be represented. Since the computational effort of *ab initio* methods scales formally as N_b^4,[30] it is important to make the basis set as small as possible without compromising the accuracy or missing part of the state space which should be represented. Hence, one purpose of this paper is to determine the effects of basis sets[39] for the calculations of Raman spectra by considering the Slater-type basis set STO-3G and split valence basis sets 3-21G, 6-31G, and 6-31G(d) (i.e., 6-31G*).

B. Vibrational analysis and Raman scattering activity

The vibrational analysis of polyatoms described by Wilson *et al.*[41] has been implemented in the GAUSSIAN 98 program. This analysis is valid only when the first derivatives of the energy with respect to the displacement of the atoms are zero (in other words, the geometry used for vibrational analysis must be optimized at the same level of theory and with the same basis set that the second derivatives are generated with). The force constant matrix **K** is defined as the second partial derivatives of the potential V with respect to the displacement of the atoms in Cartesian coordinates (for example, Δx_k, Δy_k, Δz_k of the kth atom), i.e., a $3n \times 3n$ matrix (n is the number of atoms) whose elements are given by

$$K_{ij} = \left(\frac{\partial^2 V}{\partial \eta_i \partial \eta_j}\right)_0 \quad (i,j=1,2,\ldots,3n), \quad (1)$$

where $(\eta_1, \eta_2, \eta_3) \equiv (\Delta x_1, \Delta y_1, \Delta z_1)$. $(\cdots)_0$ means that the second partial derivatives are taken at the equilibrium positions of the atoms. Usually, the matrix **K** in Cartesian coordinates is converted to a new matrix $\widetilde{\mathbf{K}}$ in mass-weighted Cartesian coordinates $q_i = m_i^{1/2}\eta_i$, i.e.,

$$\widetilde{K}_{ij} \equiv (m_i m_j)^{-1/2} K_{ij} = \left(\frac{\partial^2 V}{\partial q_i \partial q_j}\right)_0, \quad (2)$$

where m_i is the mass of the atom. Then, the eigenvalues λ_k of $\widetilde{\mathbf{K}}$ give the fundamental frequencies $\widetilde{\nu}_k$ (in the unit of cm^{-1}), i.e., $\widetilde{\nu}_k = \lambda_k^{1/2}/(2\pi c)$, where c is the velocity of light in vacuum. The eigenvectors give the normal modes.

To lowest order, Raman intensities are proportional to the derivatives of the dipole polarizability with respect to the vibrational normal modes of the material, evaluated at the equilibrium geometry. For example, most Raman scattering experiments use a plane-polarized incident laser beam. The direction of the incident beam, the polarization direction of this beam, and the direction of observation are chosen to be perpendicular to each other. Under these circumstances, the first-order differential cross section for Raman scattering in the qth vibrational mode is written as[42]

$$\left(\frac{d\sigma}{d\Omega}\right)_q = \frac{\hbar \omega_s^4}{90c^4\pi\omega_q(1-n_q)} I_{raman}. \quad (3)$$

I_{raman} is the Raman scattering activity, and $n_q = \exp[-\hbar\omega_q/(\kappa_B T)]$. ω_s is the frequency of the scattered radiation, ω_q is the frequency of the qth vibrational mode, κ_B is Boltzmann's constant, and T is temperature. For the special case of $\pi/2$ scattering geometry, I_{raman} can be written as

$$I_{raman} = 5\left(\frac{d\alpha_{xx}}{d\Xi_q} + \frac{d\alpha_{yy}}{d\Xi_q} + \frac{d\alpha_{zz}}{d\Xi_q}\right)^2 + \frac{7}{4}\left[\left(\frac{d\alpha_{xx}}{d\Xi_q} - \frac{d\alpha_{yy}}{d\Xi_q}\right)^2\right.$$
$$+ \left(\frac{d\alpha_{xx}}{d\Xi_q} - \frac{d\alpha_{zz}}{d\Xi_q}\right)^2 + \left(\frac{d\alpha_{yy}}{d\Xi_q} - \frac{d\alpha_{zz}}{d\Xi_q}\right)^2$$
$$\left.+ 6\left(\frac{d\alpha_{xy}}{d\Xi_q}\right)^2 + 6\left(\frac{d\alpha_{xz}}{d\Xi_q}\right)^2 + 6\left(\frac{d\alpha_{yz}}{d\Xi_q}\right)^2\right]^2, \qquad (4)$$

where Ξ_q is the normal coordinate corresponding to the qth vibrational mode and α is the dipole polarizability tensor. It should be mentioned that the above equation is valid only if resonant effects are neglected, and the π scattering geometry is more typical than $\pi/2$ one in the Raman measurements of a C$_{60}$ crystal.

To obtain the Raman activities, one must compute the derivatives of the polarizability with respect to the normal mode coordinates Ξ_q. These can be viewed as directional derivatives in the space of 3N nuclear coordinates and are expressed in terms of derivatives with respect to atomic coordinates, R_k. For the polarizability component α_{ij} ($i,j = x,y,z$), we have

$$\frac{d\alpha_{ij}}{d\Xi_q} = \sum_{k=1}^{3N} \frac{\partial\alpha_{ij}}{\partial R_k}\xi_{kq}, \qquad (5)$$

where $\xi_{kq} = \partial R_k/\partial\Xi_q$ is the kth atomic displacement of the qth normal mode. Then, the necessary derivatives can be expressed in terms of the atomic forces as follows:[41,42]

$$\frac{\partial\alpha_{ij}}{\partial R_k} = -\frac{\partial^3 E}{\partial G_i \partial G_j \partial R_k} = \frac{\partial^2 F_k}{\partial G_i \partial G_j}, \qquad (6)$$

where E is the total energy, G_i is the ith component of an assumed external electric field **G**, and $F_k = \partial E/\partial R_k$ is the calculated force on the kth atomic coordinate.

III. RESULTS

A. Geometry optimizations

In our previous work,[16] we calculated the bond lengths of C$_{48}$N$_{12}$ by using the B3LYP (Ref. 43) hybrid DFT method with the 6-31G basis set. The geometry of C$_{48}$N$_{12}$ is shown in Fig. 1, where the 10 unique sites (vertices 1–10) can be identified from nuclear magnetic resonance.[16] It was found that there are 15 unique types of bonds in C$_{48}$N$_{12}$ (Ref. 16): 6 nitrogen-carbon bonds and 9 carbon-carbon bonds. In contrast, C$_{60}$ has one kind of single (C—C) bond and one kind of double bond (C=C).

In this paper, we discuss the effect of basis sets using different *ab initio* methods. Before calculating the RSA's and RAF's of both C$_{60}$ and C$_{48}$N$_{12}$, we first optimize their geometries by using RHF and B3LYP hybrid DFT methods with a variety of basis sets including STO-3G, 3-21G,
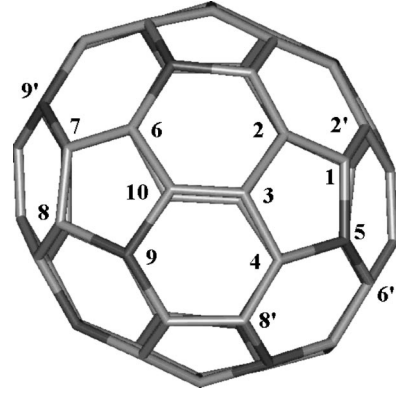

FIG. 1. C$_{48}$N$_{12}$ structure. Red is for nitrogen sites and grey for carbon sites. There are 10 unique vertices (1–10) as labeled. The 15 bonds between labeled vertices are all unique.

6-31G, and 6-31G*. The B3LYP DFT method includes a mixture of Hartree-Fock (exact) exchange, Slater local exchange,[44] Becke 88 nonlocal exchange,[45] the VWN III local exchange-correlation functional,[46] and the LYP correlation functional.[47] The optimized bond lengths for C$_{48}$N$_{12}$ and C$_{60}$ are listed in Table I. Compared to C$_{60}$, in C$_{48}$N$_{12}$ the lengths of bonds that were C$_{60}$ double bonds (for example, C1—C2′, C3—C10) increase, while the lengths of bonds that were single bonds in C$_{60}$ (for example, C3—C4, C6—C10) decrease, yielding two bonds with a small difference in length. According to our B3LYP/6-31G* calculation, the bond length difference is reduced from 0.059 Å in C$_{60}$ to 0.027–0.041 Å in C$_{48}$N$_{12}$. This can be explained by the fact that the 12 extra electrons in C$_{48}$N$_{12}$ fill t_{1u} and t_{1g} orbitals which have some antibonding character and consequently increase the length of C=C double bonds. Compared with B3LYP calculations and experiments [48] for C$_{60}$, RHF generally underestimates the lengths of C=C and C—C bonds by about 0.5%. Judging from the success of the B3LYP geometries for C$_{60}$, we conclude that the role of electron correlation is important in the accurate description of localization and delocalization of π electrons in C$_{60}$. Such bond equalization has also been observed in the DFT calculations for K$_3$C$_{60}$ by Bohnen *et al.*[49] and for C$_{60}^{-6}$ by Choi *et al.*[28] To prevent the collapse of the valence functions into the inner shell and ensure an adequate description of bonding interactions which involve overlap of valence functions, the 6-31G* basis set for carbon and nitrogen provides a better description of the inner-shell region as well as the valence region than STO-3G, 3-21G, and 6-31G basis sets.[39,50] Overall, the bond length L in C$_{60}$ or C$_{48}$N$_{12}$, as listed in Table I, follows the order: $L_{6\text{-}31G*} < L_{3\text{-}21G} < L_{6\text{-}31G} < L_{STO\text{-}3G}$, where $L_{6\text{-}31G*}$ for C$_{60}$ is in good agreement with experiment. The ordering of bond lengths suggest that increasing the flexibility of the basis from 3-21 to 6-31G favors expansion of the C$_{60}$, while the extra polarization functions in 6-31G* are needed to recontract C$_{60}$. As a result, the 3-21G basis set fortuitously gives bond lengths closer to experiment than does the bigger 6-31G basis set.

According to our DFT or RHF calculations, the diameter of C$_{48}$N$_{12}$ varies, as compared to that of C$_{60}$, from -0.3 Å

TABLE I. Bond lengths (L, in Å) in $C_{48}N_{12}$, and C_{60} calculated by using B3LYP hybrid DFT and RHF methods with STO-3G, 3-21G, 6-31G and 6-31G* basis sets. i and j in Ci and Nj are the site numbers labeled in Fig. 1. The symbols "C—C" and "C=C" in parentheses denote the original single and double bonds in C_{60}. The averaged bond length $L_{ave} = (L_{C=C} + 2L_{C-C})/3$.

| Fullerene | Bond | STO-3G | | 3-21G | | 6-31G | | 6-31G* | | Expt. |
		L_{dft}	L_{rhf}	L_{dft}	L_{rhf}	L_{dft}	L_{rhf}	L_{dft}	L_{rhf}	Ref. 48
$C_{48}N_{12}$	C1—C2′ (C=C)	1.437	1.415	1.417	1.408	1.422	1.413	1.416	1.402	
	C1—C2 (C—C)	1.428	1.391	1.410	1.386	1.413	1.388	1.406	1.384	
	C1—N5 (C—C)	1.474	1.460	1.432	1.421	1.432	1.416	1.430	1.427	
	C3—C2 (C—C)	1.470	1.466	1.452	1.452	1.449	1.448	1.446	1.452	
	C3—C4 (C—C)	1.409	1.359	1.395	1.362	1.397	1.365	1.390	1.359	
	C3—C10 (C=C)	1.456	1.457	1.432	1.435	1.434(6)	1.437	1.431(4)	1.436(8)	
	C4—C8′ (C=C)	1.457	1.459	1.433	1.437	1.435(4)	1.439	1.431(3)	1.437(2)	
	C4—N5 (C—C)	1.471	1.455	1.431	1.413	1.429	1.411	1.422	1.405	
	N5—C6′ (C=C)	1.475	1.464	1.430	1.429	1.432	1.428	1.429	1.431	
	C6—C10 (C—C)	1.412	1.364	1.396	1.366	1.400	1.371	1.394	1.363	
	C6—C7 (C—C)	1.440	1.435	1.421	1.418	1.422	1.419	1.414	1.414	
	C7—C8 (C—C)	1.420	1.371	1.402	1.372	1.407	1.376	1.402	1.370	
	C7—N9′ (C=C)	1.459	1.442	1.416	1.405	1.419	1.407	1.410	1.396	
	C8—N9 (C—C)	1.451	1.431	1.418	1.408	1.415	1.401	1.408	1.406	
	N9—C10 (C—C)	1.461	1.436	1.427	1.404	1.423	1.399	1.413	1.392	
C_{60}	C=C (C1—C2′)	1.413	1.376	1.390	1.367	1.398	1.375	1.395	1.373	1.391
	C—C (C1—C2,C1—C5)	1.477	1.463	1.460	1.453	1.459	1.452	1.454	1.449	1.455
	L_{ave}	1.456	1.434	1.437	1.424	1.439	1.426	1.434	1.424	1.434

to $+0.2$ Å, which has a strong effect on the force constant that determines the frequencies of the vibrational modes of molecule. Hence, we expect that the vibrational frequencies of $C_{48}N_{12}$ will be strongly influenced by the bond equalization effects and the expansion and contraction of the ball. In the following, we investigate the vibrational properties of $C_{48}N_{12}$ and C_{60} based on the optimized geometries.

B. Raman-active vibrational frequencies

Using the GAUSSIAN 98 program,[39,40] we calculated the RAF's of both C_{60} and $C_{48}N_{12}$. We compare with C_{60} experiment to determine the effects of electron correlations and basis sets. It should be mentioned that our frequencies have not been scaled.

Table II summarizes the calculated results for C_{60} obtained by using RHF and B3LYP hybrid DFT methods. As shown by Dresselhaus et al.,[51] there are 46 different vibrational modes in the 174 independent normal vibrations of C_{60}. These modes are classified in even and odd parities and in the 10 irreducible representatives of the I_h point group:[51] the $\{a_g, a_u\}$, $\{t_{1g}, t_{1u}, t_{2g}, t_{2u}\}$, $\{g_g, g_u\}$, and $\{h_g, h_u\}$ modes are non-, threefold-, fourfold- and fivefold-degenerate, respectively. Among the 46 vibrational modes are 10 Raman-active ones. In choosing a basis set for the first-principles calculation, one must make a compromise between accuracy and CPU time. Table II shows that the minimum calculation can be done in about 5 h of CPU, while the most expensive calculation requires 21 days of CPU. Without significant computational cost, one can do B3LYP/STO-3G calculations and still obtain results more accurate than any RHF calculations. Going beyond STO-3G for

B3LYP cases requires a drastic increase in CPU time. Suprisingly, going just to 3-21G provides the most accurate results, while for the bigger basis set 6-31G, the results are worse and adding a polarized function to 6-31G only slightly improves the results. The 3-21G basis set gives systematically lower frequencies than the 6-31G basis set, while the frequencies obtained from the 6-31G* basis set typically lie in between the results of the other two basis sets. In contrast, 6-31G* does provide the most accurate bond lengths. This suggests that the better accuracy of 3-21G is fortuitous. Increasing the basis set to 6-31G stiffens the bonds, while adding the polarization function compensates by softening the bonds. In comparison with the B3LYP results, RHF-calculated frequencies are too high due to an incorrect description of bond dissociation which leads to an increased force constant, while B3LYP's with large basis sets are generally in good agreement with the experiments of Wang et al.[21] In comparison with both effects, we find that the correlation effect on the RAF's is stronger than the basis set effect. This demonstrates the importance of electron correlation in the accurate description of the vibrational frequencies of these molecules.

For comparison, Table III lists the calculated vibrational frequencies of C_{60} obtained by using various theories, for example, the semiempirical MNDO (Ref. 52) and QCFF/PI (Ref. 53) methods. Of these, the QCFF/PI method, which has been parametrized mainly with respect to vibrational frequencies of conjugated and aromatic hydrocarbons,[54] results in the best results although it gives less satisfactory geometry. Such an accurate prediction implies that the electronic structure of C_{60} is not much different from other aromatic hydrocarbons.[53] Häser et al.[33] showed that the approximate

TABLE II. RHF and B3LYP hybrid DFT calculations of Raman scattering activities (I_{raman}, in 10^{-14} m^4/kg) of C$_{60}$ with the corresponding vibrational modes and frequencies ν (cm^{-1}). h_g and a_g modes are unpolarized and polarized, respectively. Numbers in the parentheses are the relative errors between the calculated and the experimental frequencies ν^{exp} (see Table III) of Wang *et al.* (Ref. 23). The approximated CPU time for each case at the Sun64/SVR4 Unix system (4 processors) is also listed.

Method	Mode	STO-3G		3-21G		6-31G		6-31G*	
		I_{raman}	ν	I_{raman}	ν	I_{raman}	ν	I_{raman}	ν
RHF	a_g	3894	1684 (14.6%)	3467	1604 (9.2%)	3840	1637 (11.4%)	3968	1600 (8.9%)
		441	553 (21.1%)	488	518 (5.0%)	558	526 (6.8%)	574	527 (6.4%)
	h_g	255	1912 (21.6%)	224	1772 (12.7%)	279	1799 (14.4%)	283	1791 (13.9%)
		34	1658 (16.3%)	35	1546 (8.4%)	38	1585 (11.1%)	22	1562 (9.5%)
		188	1482 (18.7%)	215	1326 (6.2%)	199	1377 (10.3%)	210	1380 (10.6%)
		87	1290 (17.4%)	76	1184 (7.7%)	44	1208 (9.9%)	105	1208 (9.9%)
		38	886 (14.6%)	38	828 (7.2%)	5	843 (9.0%)	46	840 (8.7%)
		11	836 (18.1%)	16	761 (7.5%)	5	821 (15.9%)	9	794 (12.2%)
		14	509 (18.0%)	19	475 (10.2%)	16	496 (14.9%)	12	482 (11.9%)
		75	302 (11.9%)	111	295 (9.2%)	116	296 (9.5%)	115	289 (7.1%)
CPU Time		5 h		12 h		20 h		36 h	
B3LYP	a_g	3008	1549 (5.4%)	2643	1501 (2.1%)	2758	1524 (3.7%)	2760	1504 (2.4%)
		654	502 (1.9%)	681	491 (0.4%)	750	496 (0.6%)	724	489 (0.8%)
	h_g	320	1677 (6.6%)	297	1609 (2.3%)	325	1627 (3.4%)	312	1618 (2.8%)
		28	1500 (5.2%)	18	1436 (0.7%)	23	1466 (2.8%)	19	1455 (2.0%)
		138	1332 (6.7%)	168	1231 (1.4%)	151	1274 (2.1%)	170	1275 (2.1%)
		74	1166 (6.1%)	71	1112 (1.2%)	75	1129 (2.8%)	71	1125 (2.4%)
		47	802 (3.8%)	48	781 (1.1%)	44	788 (1.9%)	48	766 (0.9%)
		4	734 (3.7%)	5	678 (4.3%)	4	738 (4.3%)	5	718 (1.4%)
		4	449 (4.2%)	5	429 (0.5%)	4	448 (3.9%)	5	436 (1.2%)
		95	271 (0.5%)	128	271 (0.3%)	135	272 (0.2%)	130	266 (1.7%)
CPU Time		21 h		5 days		7.5 days		21 days	

TABLE III. The vibrational frequencies obtained by other theoretical calculations performed by Choi *et al.* (Ref. 28), Bohnen *et al.* (Ref. 49), Stanton *et al.* (Ref. 52), Negri *et al.* (Ref. 53), Jishi *et al.* (Ref. 58), Dixon *et al.* (Ref. 59), Hara *et al.* (Ref. 60), and Onida *et al.* (Ref. 61). Numbers in the parentheses are the relative errors to the experimental frequencies ν^{expt}, of Wang *et al.* (Ref. 23).

SIFC [a]	LDA [b]	LDA [c]	LDA [d]	[e]CPMD	QCFF/PI [f]	MFCM [g]	MNDO [h]	Expt. [i]
a_g								
1474 (0.3%)	1531 (4.2%)	1525 (3.8%)	1475 (0.4%)	1447 (1.5%)	1442 (1.8%)	1468 (0.1%)	1667 (13.5%)	1469
484 (1.8%)	502 (1.8%)	499 (1.2%)	481 (2.4%)	482 (2.2%)	513 (4.1%)	492 (0.2%)	610 (23.7%)	493
h_g								
1582 (0.6%)	1609 (2.3%)	1618 (2.8%)	1580 (0.4%)	1573 (0.0%)	1644 (4.5%)	1575 (0.1%)	1722 (9.5%)	1573
1419 (0.5%)	1475 (3.4%)	1475 (3.4%)	1422 (0.3%)	1394 (2.2%)	1465 (2.7%)	1401 (1.8%)	1596 (11.9%)	1426
1250 (0.2%)	1288 (3.2%)	1297 (3.9%)	1198 (4.0%)	1208 (3.2%)	1265 (1.4%)	1217 (2.5%)	1407 (12.7%)	1248
1117 (1.6%)	1129 (2.7%)	1128 (2.6%)	1079 (1.8%)	1098 (0.1%)	1154 (5.0%)	1102 (0.3%)	1261 (14.7%)	1099
782 (1.2%)	794 (2.7%)	788 (1.9%)	763 (1.3%)	775 (0.3%)	801 (3.6%)	788 (1.9%)	924 (19.5%)	773
704 (0.6%)	711 (0.4%)	727 (2.7%)	716 (1.1%)	730 (3.1%)	691 (2.4%)	708 (0.0%)	771 (8.2%)	708
436 (1.2%)	430 (0.2%)	431 (0.0%)	422 (2.1%)	435 (0.9%)	440 (2.1%)	439 (1.9%)	447 (3.7%)	431
272 (0.7%)	269 (0.4%)	261 (3.3%)	263 (2.6%)	261 (3.3%)	258 (4.4%)	269 (0.4%)	263 (2.7%)	270

[a]Reference 28.   [f]Reference 53.
[b]Reference 60.   [g]Reference 58.
[c]Reference 59.   [h]Reference 52.
[d]Reference 49.   [i]Reference 23.
[e]Reference 61.

harmonic frequencies for the two a_g vibrational modes of C_{60} are 1615 cm^{-1} (9.9%) and 487 cm^{-1} (1.2%) at HF/DZP, 1614 cm^{-1} (9.9%) and 483 cm^{-1} (2.0%) at HF/TZP, 1614 (9.9%) cm^{-1} and 437 (12.2%) cm^{-1} at MP2/DZP, and 1586 (7.9%) cm^{-1} and 437 (12.2%) cm^{-1} at MP2/TZP, where the percentages in the parentheses are the relative errors of the calculated results to the experimental frequencies obtained by Wang *et al.*[23] Their HF calculations are in agreement with our RHF/3-21G results. Their MP2 results are more accurate when obtained with large basis sets, which also demonstrates the importance of electron correlation in predicting accurately the vibrational frequencies of a molecule.

In addition, a number of force-constant models (FCM's) that include interactions up to the second-nearest neighbors[55–57] are used to calculate the vibrational frequencies of C_{60}. None of them yield good agreement with the experiment data. For example, an empirical force field, which has been parametrized with respect to polycyclic aromatic hydrocarbons, is used with the Hückel theory and predicts that the vibrational frequencies of the two a_g modes are 1409 cm^{-1} and 388 cm^{-1},[56] which are too low. However, the modified FCM (MFCM) by Jishi *et al.*[58] considered interactions up to the third-nearest neighbors. The results obtained by using the MFCM,[58] as shown in Table III, are in excellent agreement with the experiments of Wang *et al.*[23]

Table III also lists the calculated vibrational frequencies of C_{60} obtained by other DFT methods, for example, local density approximation[49,59,60] (LDA) and DFT-LDA-based Car-Parrinello molecular dynamics (CPMD) simulation.[61] In general, those calculated results are in good agreement with experiment.

Recently, Choi *et al.*[28] have performed B3LYP vibrational calculations of C_{60} with a 3-21G basis set but involving scaling of the internal force constants (SIFC) $\widetilde{K}_{ij}^{int}$ by using the method of Pulay *et al.*,[62] i.e.,

$$\widetilde{K}_{ij}^{scaled} = (s_i s_j)^{1/2} \widetilde{K}_{ij}^{int}, \tag{7}$$

where $\widetilde{K}_{ij}^{int}$ is the force constant in internal coordinates (the GAUSSIAN 98 program[39] uses this form), and s_i and s_j are scaling factors for the ith and jth redundant internal coordinates, respectively. They optimized the scaling factors by minimizing the root-mean-square deviations between the experimental and calculated scaled frequencies. Their results are also listed in Table III. Their scaling procedure does improve the accuracy for the 10 Raman-active vibrational frequencies of C_{60}.

It should be mentioned that although vibrational calculations are all done for an isolated C_{60} molecule, the calculated results are usually compared to experimental data on C_{60} molecular vibrations in the solid state, in the gas phase or in solution. The theoretical justification for this lies in the weak van der Waals bonds between C_{60} molecules.[5] The comparison between the observed vibrational spectra of C_{60} (Ref. 5) demonstrated that the measured mode frequencies are

TABLE IV. Fifty-eight Raman-active frequencies ν (cm^{-1}) for $C_{48}N_{12}$ calculated by using RHF method with STO-3G, 3-21G, 6-31G, and 6-31G* basis sets.

Doubly degenerate modes				Nondegenerate modes			
STO-3G	3-21G	6-31G	6-31G*	STO-3G	3-21G	6-31G	6-31G*
262.9	262.1	268.3	260.7	293.9	287.6	291.2	287.9
285.8	280.9	285.5	280.8	444.6	406.1	428.9	387.5
429.1	408.9	427.5	412.9	462.5	415.1	447.6	424.5
470.4	433.3	454.6	440.1	510.2	455.2	483.2	454.0
513.6	478.7	496.7	488.3	522.6	490.8	511.4	488.6
583.2	516.9	548.6	539.9	575.6	520.8	542.8	523.7
603.5	609.5	611.3	592.2	608.3	566.1	586.8	575.2
651.8	647.3	649.5	628.6	645.7	637.1	639.7	614.7
725.4	698.9	736.4	706.2	650.4	650.6	652.2	636.8
773.4	726.4	759.2	740.9	723.1	654.8	670.3	651.8
780.2	761.6	785.1	757.4	744.2	705.2	748.8	716.4
831.2	775.8	806.9	788.0	777.3	759.7	783.6	738.3
848.0	820.3	833.4	820.8	831.6	778.6	802.4	772.8
870.7	843.6	852.5	840.1	866.8	824.8	836.1	819.0
934.6	942.6	943.5	917.9	923.6	918.4	919.0	897.0
961.3	974.4	965.8	932.8	952.9	964.6	955.7	916.2
1238.4	1159.9	1191.9	1164.4	1216.2	1164.9	1192.3	1174.7
1280.9	1196.7	1225.0	1214.5	1327.5	1243.7	1264.1	1251.1
1313.3	1238.4	1261.7	1249.9	1344.1	1259.7	1281.3	1272.8
1422.9	1276.3	1324.6	1317.6	1400.2	1335.0	1374.0	1347.6
1476.0	1340.6	1382.7	1377.4	1468.7	1347.1	1389.0	1376.6
1546.2	1420.7	1456.9	1448.6	1498.2	1374.6	1424.4	1380.0
1608.0	1468.3	1517.1	1503.4	1533.9	1414.9	1468.7	1429.1
1647.0	1490.0	1537.2	1540.1	1583.4	1436.5	1485.1	1475.9
1716.5	1541.4	1591.4	1586.5	1655.1	1527.5	1578.0	1551.9
1780.9	1631.3	1670.8	1663.5	1721.2	1559.5	1612.3	1602.1
1831.0	1669.5	1709.9	1719.9	1766.4	1612.4	1648.6	1625.7
1882.8	1707.7	1749.3	1758.7	1817.4	1643.5	1686.6	1680.1
1915.5	1735.1	1777.7	1788.1	1946.3	1766.7	1803.8	1808.7

slightly different from one phase to another, showing that the interaction between C_{60} molecules is weak.

In Tables IV and V, we list the RAF's for $C_{48}N_{12}$ calculated with the RHF and B3LYP hybrid DFT methods, respectively, and different basis sets. In contrast with C_{60}, we find that there are in total 116 different vibrational modes[16] for $C_{48}N_{12}$ because of its lower symmetry, S_6.[16] These vibrational modes are classified in 58 doubly degenerate and 58 nondegenerate modes. Among those vibrational modes, there are 58 IR-active vibrational modes[16] and 58 Raman-active modes including 29 doubly degenerate and 29 nondegenerate ones as listed in Tables IV and V. Similar to C_{60}, including the electron correlation and increasing the basis size leads to a redshift of the RAF's of $C_{48}N_{12}$. From our calculated results, we find that the nitrogen-substitutional doping results in a symmetry lowering and an increase in the reduced mass. The symmetry lowering splits some of the degenerate vibrational modes observed in C_{60} and makes many more modes Raman-active for $C_{48}N_{12}$. Overall, the increase of the reduced mass redshifts the vibrational frequencies of C_{60}.

TABLE V. Fifty-eight Raman-active frequencies ν (cm^{-1}) for $C_{48}N_{12}$ calculated by using B3LYP hybrid DFT methods with STO-3G, 3-21G, 6-31G, and 6-31G* basis sets.

Doubly degenerate modes				Nondegenerate modes			
STO-3G	3-21G	6-31G	6-31G*	STO-3G	3-21G	6-31G	6-31G*
245.1	247.7	252.1	245.1	263.8	264.3	267.5	263.6
258.9	261.1	264.5	259.5	381.9	368.2	389.4	376.2
376.1	367.7	386.7	371.2	405.7	397.7	415.0	398.3
410.2	388.2	408.9	396.0	444.4	415.4	441.7	423.8
446.7	428.7	446.2	436.5	471.2	458.4	477.3	466.6
492.6	449.5	482.0	471.6	498.3	490.5	500.2	494.9
548.8	567.5	566.0	551.1	544.1	504.5	544.2	510.0
580.3	596.3	596.8	580.6	577.5	588.2	592.1	575.7
617.3	612.8	652.2	626.6	585.2	597.8	601.5	588.1
649.4	629.1	662.4	641.2	621.0	603.0	616.3	596.9
665.2	670.6	698.1	671.1	624.9	614.1	652.1	627.0
715.9	695.0	713.9	698.6	657.8	657.1	684.2	656.2
766.6	760.4	768.0	765.8	729.5	690.1	709.4	688.5
781.7	776.0	782.4	779.7	768.2	764.8	772.5	765.5
840.8	865.3	860.2	842.6	835.5	850.5	844.4	829.7
858.1	887.4	876.6	853.9	855.9	881.0	868.6	843.7
1123.7	1084.4	1104.9	1092.7	1114.7	1079.8	1099.8	1092.1
1162.2	1122.8	1140.6	1138.0	1193.6	1160.0	1172.5	1161.6
1181.5	1146.8	1162.9	1155.8	1220.7	1181.4	1195.8	1189.0
1274.1	1186.0	1220.0	1222.6	1315.9	1240.9	1267.3	1265.1
1318.1	1243.4	1273.6	1271.7	1337.1	1253.2	1280.2	1279.0
1386.2	1310.8	1336.6	1336.3	1366.7	1292.5	1322.1	1319.8
1451.9	1369.3	1406.8	1404.1	1416.4	1346.6	1382.6	1378.9
1466.1	1387.9	1420.4	1419.7	1438.7	1372.8	1414.5	1397.4
1503.9	1415.3	1451.6	1451.0	1481.0	1418.8	1453.2	1441.1
1570.8	1488.6	1516.8	1515.4	1530.7	1440.4	1477.2	1476.6
1595.2	1516.0	1550.6	1551.0	1558.4	1487.1	1511.4	1505.3
1633.1	1544.0	1577.6	1577.8	1580.5	1508.5	1545.1	1530.4
1661.7	1577.6	1609.8	1609.8	1682.7	1592.0	1623.7	1622.9

C. Raman scattering activities

In this paper, we only calculate nonresonant Raman intensities. We performed *ab initio* calculations of Raman scattering activities I_{raman} (Refs. 17,18) for the optimized geometries of $C_{48}N_{12}$ and C_{60} by using the GAUSSIAN 98 program [39,40] with RHF and B3LYP hybrid DFT methods.

To test the basis set dependence of the theoretical RSA's, calculations for basis sets of different sizes have been performed for C_{60}. In Table II are listed the RSA's for C_{60} calculated with STO-3G, 3-21G, 6-31G, and 6-31G*. For each basis set, the strongest Raman-active lines of C_{60} are the two a_g modes, which is consistent with Raman experiments.[20–24] The a_g modes are identified by their polarized character, which strongly suggests that both a_g modes are totally symmetric.[51] The remaining 8 Raman-active modes are unpolarized, consistent with the fivefold-degenerate h_g symmetry.[51] Also, we find that electron correlation and basis set change significantly the RSA of a given Raman-active mode. However, the correlation effect is stron-
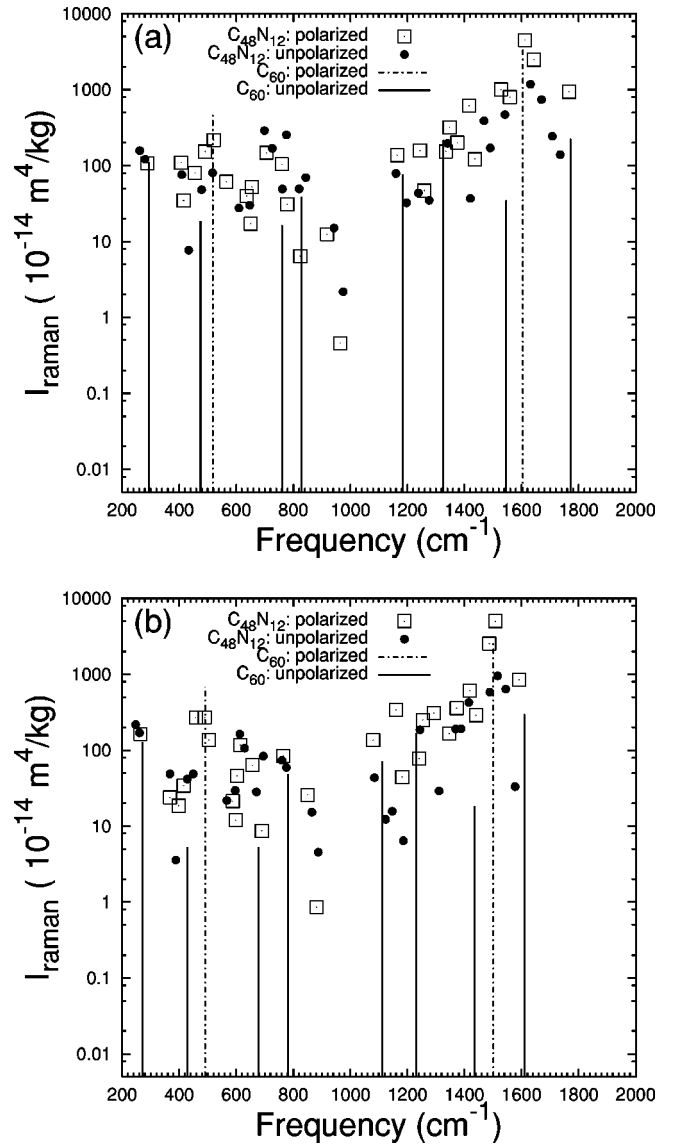

FIG. 2. *Ab initio* calculations of Raman scattering activities (I_{raman}, in 10^{-14} m^4/kg) in $C_{48}N_{12}$ with (a) RHF/3-21G and (b) B3LYP/3-21G. Open squares and solid circles are nondegenerate polarized and doubly degenerate unpolarized Raman-active modes, respectively, for $C_{48}N_{12}$. The solid and dot-dashed lines are the calculated unpolarized and polarized Raman spectral lines of C_{60}, respectively.

ger than the basis set effect. In general, electron correlation reduces the RSA of the strongest Raman-active a_g mode of C_{60} by about 25%. For other specific Raman-active modes, the electron correlation predicts at least a 20% decrease (or increase) of the RSA obtained by the RHF method. Increasing the size of the basis set from STO-3G to 6-31G results in about a 10% decrease (or increase) of the RSA, while adding polarization functions leads to about a 3% decrease (or increase) of the RSA. For a specific mode (for example, the qth one), we find that the kth atomic displacement ξ_{kq} of this mode changes little as we choose different basis sets and/or consider the electron correlation. Thus, according to Eq. (5), the RSA mainly depends on the derivative of the polarizabil-

ity α with respect to atomic coordinates R, which are related to the choice of basis sets and the inclusion of electron correlations.

In Figs. 2(a) and 2(b), we show the calculated RSA's I_{raman} at the corresponding RAF's ν for $C_{48}N_{12}$ by using RHF/3-21G and B3LYP/3-21G, respectively. We find that the Raman spectrum of $C_{48}N_{12}$ separates into two regions, i.e., high-frequency (1100–1700 cm^{-1}) and low-frequency (200–1000 cm^{-1}) regions, which are similar to those of C_{60}. In detail, this aza-fullerene, unlike C_{60}, has an equal number of polarized and unpolarized Raman-active modes in each region and, in particular, has 6 more Raman-active modes in the low-frequency region than in the high-frequency one. The strongest Raman spectral lines in both low- and high-frequency regions are the nondegenerate polarized ones located at 1509 cm^{-1} and 491 cm^{-1}, respectively, which are almost the same as those of the strongest a_g modes of C_{60}. As shown in Fig. 2, the lowest and highest RAF's of $C_{48}N_{12}$ are almost the same as those of C_{60}. Comparing Fig. 2(a) with Fig. 2(b) shows that the RAF's of $C_{48}N_{12}$ predicted by RHF method, as discussed above, are redshifted due to electron correlations. The effects of basis set and electron correlations on RSA's of $C_{48}N_{12}$ are similar to those obtained for C_{60}. Detailed analysis of Raman-active vibrational modes of $C_{48}N_{12}$ shows that (i) the Raman spectra in the high-frequency region ($>$1400 cm^{-1}) come mainly from carbon-carbon vibrations, (ii) the strong nitrogen-carbon vibrations occur only in the low-frequency region, and (iii) the strongest and weakest Raman signals come from the contributions of carbon-carbon vibrations.

IV. SUMMARY

In summary, we have performed large-scale *ab initio* calculations of RSA's and RAF's in $C_{48}N_{12}$ as well as C_{60} using B3LYP hybrid DFT and RHF methods. We predict that $C_{48}N_{12}$ has 29 nondegenerate polarized and 29 doubly degenerate unpolarized RAF's, and the RAF of the strongest spectral lines in the low- and high-frequency regions and the lowest and highest RAF's are almost the same as those of C_{60}. The 10 RAF's of C_{60} calculated with the B3LYP hybrid DFT method and large basis set are in excellent agreement with experiment. Our study of C_{60} reveals the importance of electron correlations and basis sets in *ab initio* calculations, and our calculated Raman results of C_{60} demonstrate the desirable efficiency and accuracy of the B3LYP hybrid DFT method for obtaining important quantitative information on the vibrational properties of these fullerenes. Finally, we hope that these calculations will provide an incentive for Raman measurements of $C_{48}N_{12}$.

*Corresponding author. Email address: rhxie@nist.gov

[1] H. W. Kroto, J. R. Heath, S. C. O'Brien, R. F. Curl, and R. E. Smalley, Nature (London) **318**, 162 (1985).

[2] R. F. Curl and R. E. Smalley, Sci. Am. **264**, 54 (1991).

[3] W. Krätschmer, L. D. Lamb, K. Fostiropoulos, and D. R. Huffman, Nature (London) **347**, 354 (1990).

[4] D. R. Huffman, Phys. Today **44**(X), 22 (1991).

[5] M. S. Dresselhaus, G. Dresselhaus, and P. C. Eklund, *Science of Fullerenes and Carbon Nanotubes* (Academic Press, New York, 1996).

[6] *The Physics of Fullerene-Based and Fullerene-Related Materials*, edited by W. Andreoni (Kluwer, New York, 2000).

[7] R. H. Xie, in *Nonlinear Optical Materials, Vol. 9 of Handbook of Advanced Electronic and Photonic Materials and Devices*, edited by H. S. Nalwa (Academic Press, New York, 2000), pp. 267–307; R. H. Xie, Q. Rao, and L. Jensen, in *Encyclopedia of Nanoscience and Nanotechnology*, edited by H. S. Nalwa (American Scientific, Stevenson Ranch, CA, 2003).

[8] R. H. Xie, Chem. Phys. Lett. **310**, 379 (1999); R. H. Xie and Q. Rao, Appl. Phys. Lett. **72**, 2358 (1998); R. H. Xie and J. Jiang, Appl. Phys. Lett. **71**, 1029 (1997).

[9] *Perspectives of Fullerene Nanotechnology*, edited by E. Osawa (Kluwer, New York, 2002).

[10] H. M. Lee, M. M. Olmstead, E. Iezzi, J. C. Duchamp, H. C. Dorn, and A. L. Balch, J. Am. Chem. Soc. **124**, 3494 (2002).

[11] T. Guo, C. M. Jin, and R. E. Smalley, J. Phys. Chem. **95**, 4948 (1991).

[12] J. C. Hummelen, B. Knight, J. Pavlovich, R. González, and F. Wudl, Science **269**, 1554 (1995).

[13] W. Andreoni, A. Curioni, K. Holczer, K. Prassides, M. Keshavarz-K, J. C. Hummelen, and F. Wudl, J. Am. Chem. Soc. **118**, 11335 (1996).

[14] L. Hultman, S. Stafström, Z. Czigány, J. Neidhardt, N. Hellgren, I. F. Brunell, K. Suenaga, and C. Cooliex, Phys. Rev. Lett. **87**, 225503 (2001).

[15] S. Stafström, L. Hultman, and N. Hellgren, Chem. Phys. Lett. **340**, 227 (2001).

[16] R. H. Xie, G. W. Bryant, and V. H. Smith, Jr., Chem. Phys. Lett. **368**, 486 (2003).

[17] L. A. Woodward, *Introduction to the Theory of Molecular Vibrations and Vibrational Spectroscopy* (Oxford University Press, London, 1972).

[18] N. B. Colthup, L. H. Daly, and S. E. Wiberley, *Introduction to Infrared and Raman Spectroscopy*, 3rd ed. (Academic Press, New York, 1990).

[19] W. Krätschmer, K. Fostiropoulos, and D. R. Huffman, Chem. Phys. Lett. **170**, 167 (1990).

[20] D. S. Bethune, G. Meijer, W. C. Tang, H. J. Rosen, W. G. Golden, H. Seki, C. A. Brown, and M. S. de Vries, Chem. Phys. Lett. **179**, 181 (1991).

[21] K. A. Wang, A. M. Rao, P. C. Eklund, M. S. Dresselhaus, and G. Dresselhaus, Phys. Rev. B **48**, 11 375 (1993).

[22] M. C. Martin, X. Du, J. Kwon, and L. Mihaly, Phys. Rev. B **50**, 173 (1994).

[23] K. A. Wang, Y. Wang, P. Zhou, J. M. Holden, S. L. Ren, G. T. Hager, H. F. Ni, P. C. Eklund, G. Dresselhaus, and M. S. Dresselhaus, Phys. Rev. B **45**, R1955 (1992).

[24] K. Lynch, C. Tanke, F. Menzel, W. Brockner, P. Scharff, and E. Stumpp, J. Phys. Chem. **99**, 7985 (1995).

[25] P. Zhou, K. A. Wang, Y. Wang, P. C. Eklund, M. S. Dresselhaus, G. Dresselhaus, and R. A. Jishi, Phys. Rev. B **46**, 2595 (1992); S. Guha, J. Menéndez, J. B. Page, G. B. Adams, G. S. Spencer, J. P. Lehman, P. Giannozzi, and S. Baroni, Phys. Rev. Lett. **72**, 3359 (1994); P. J. Horoyski, M. L. W. Thewalt, and T. R. Anthony, *ibid.* **74**, 194 (1995); P. Giannozzi and W. Andreoni, *ibid.* **76**, 4915 (1996); K. Pokhodnia, J. Demsar, A. Omerzu, D. Mihailovic, and H. Kuzmany, *ibid.* **55**, 3757 (1997); M. F. Limonov, Yu. E. Kitaev, A. V. Chugreev, V. P. Smirnov, Yu. S. Grushko, S. G. Kolesnik, and S. N. Kolesnik, *ibid.* **57**, 7586 (1998); X. H. Chen, T. Takenobu, T. Muro, H. Fudo, and Y. Iwasa, *ibid.* **60**, 12 462 (1999); V. A. Davydov, L. S. Kashevarova, A. V. Rakhmanina, V. M. Senyavin, R. Céolin, H. Szwarc, H. Allouchi, and V. Agafonov, *ibid.* **61**, 11 936 (2000); I. D. Hands, J. L. Dunn, and C. A. Bates, *ibid.* **63**, 245414 (2001); A. V. Talyzin, L. S. Dubrovinsky, T. Le Bihan, and U. Jansson, *ibid.* **65**, 245413 (2002).

[26] Z. H. Dong, P. Zhou, J. M. Holden, P. C. Eklund, M. S. Dresselhaus, and G. Dresselhaus, Phys. Rev. B **48**, R2862 (1993).

[27] A. M. Rao, P. C. Eklund, S. Bandow, A. Thess, and R. E. Smalley, Nature (London) **388**, 257 (1997); A. M. Rao, E. Richter, S. Bandow, B. Chase, P. C. Eklund, K. A. Williams, S. Fang, K. R. Subbaswamy, M. Menon, A. Thess, R. E. Smalley, G. Dresselhaus, and M. S. Dresselhaus, Science **275**, 187 (1997); K. A. Williams, B. K. Pradhan, P. C. Eklund, M. K. Kostov, and M. W. Cole, Phys. Rev. Lett. **88**, 165502 (2002), and references therein.

[28] C. H. Choi, M. Kertesz, and L. Mihaly, J. Phys. Chem. A **104**, 102 (2000).

[29] J. Cioslowski, *Electronic Structure Calculations on Fullerenes and Their Derivatives* (Oxford University Press, New York, 1995); G. E. Scuseria, Science **271**, 942 (1996).

[30] D. B. Cook, *Handbook of Computational Quantum Chemistry* (Oxford University Press, New York, 1998).

[31] P. R. Taylor, E. Bylaska, J. H. Weare, and R. Kawai, Chem. Phys. Lett. **235**, 558 (1995).

[32] N. Kurita, K. Kobayashi, H. Kumahora, and K. Tago, Phys. Rev. B **48**, 4850 (1993).

[33] M. Häser, J. Almlöf, and G. E. Scuseria, Chem. Phys. Lett. **181**, 497 (1991).

[34] D. Bakowies, M. Bühl, and W. Thiel, Chem. Phys. Lett. **247**, 491 (1995).

[35] J. Cioslowski, N. Rao, and D. Moncrieff, J. Am. Chem. Soc. **124**, 8485 (2002).

[36] G. E. Scuseria, Chem. Phys. Lett. **243**, 193 (1995).

[37] D. L. Strout and G. E. Scuseria, J. Chem. Phys. **102**, 8448 (1995).

[38] P. Hohenberg and W. Kohn, Phys. Rev. **136**, B864 (1964); W. Koha and L. J. Sham, Phys. Rev. **140**, A1133 (1965).

[39] M. J. Frisch, G. W. Trucks, H. B. Schlegel, G. E. Scuseria, M. A. Robb, J. R. Cheeseman, V. G. Zakrzewski, J. A. Montgomery, Jr., R. E. Stratmann, J. C. Burant, S. Dapprich, J. M. Millam, A. D. Daniels, K. N. Kudin, M. C. Strain, O. Farkas, J. Tomasi, V. Barone, M. Cossi, R. Cammi, B. Mennucci, C. Pomelli, C. Adamo, S. Clifford, J. Ochterski, G. A. Petersson, P. Y. Ayala, Q. Cui, K. Morokuma, D. K. Malick, A. D. Rabuck, K. Raghavachari, J. B. Foresman, J. Cioslowski, J. V. Ortiz, A. G. Baboul, B. B. Stefanov, G. Liu, A. Liashenko, P. Piskorz, I. Komaromi, R. Gomperts, R. L. Martin, D. J. Fox, T. Keith, M. A. Al-Laham, C. Y. Peng, A. Nanayakkara, M. Challacombe, P. M. W. Gill, B. Johnson, W. Chen, M. W. Wong, J. L. Andres, C. Gonzalez, M. Head-Gordon, E. S. Replogle, and J. A. Pople, computer code GAUSSIAN 98, revision A.9, Gaussian, Inc., Pittsburgh, PA, 1998.

[40] Use of this software does not constitute an endorsement or certification by NIST.

[41] E. B. Wilson, J. C. Decius, and P. C. Cross, *Molecular Vibrations* (McGraw-Hill, New York, 1955).

[42] M. Cardona, in *Light Scattering in Solids II*, edited by M. Cardona, Topics in Applied Physics, Vol. 50 (Springer, Berlin, 1982).

[43] A. D. Becke, J. Chem. Phys. **98**, 5648 (1993).

[44] J. C. Slater, Phys. Rev. **81**, 385 (1951).

[45] A. D. Becke, Phys. Rev. A **38**, 3098 (1988).

[46] S. H. Vosko, L. Wilk, and M. Nusair, Can. J. Phys. **58**, 1200 (1980).

[47] C. Lee, W. Yang, and R. G. Parr, Phys. Rev. B **37**, 785 (1988).

[48] W. I. F. David, R. M. Ibberson, J. C. Matthewman, K. Prassides, T. J. S. Dennis, J. P. Hare, H. W. Kroto, R. Taylor, and D. R. M. Walton, Nature (London) **353**, 147 (1991); H. B. Bürgi, E. Blanc, D. Schwarzenbach, S. Liu, Y. Lu, M. M. Kappes, and J. A. Ibers, Angew. Chem. Int. Ed. Engl. **41**, 640 (1992).

[49] K. P. Bohnen, R. Heid, K. M. Ho, and C. T. Chan, Phys. Rev. B **51**, 5805 (1995).

[50] W. J. Hehre and J. A. Pople, J. Chem. Phys. **56**, 4233 (1972); M. S. Gordon, J. S. Binkley, J. A. Pople, W. J. Pietro, and W. J. Hehre, J. Am. Chem. Soc. **104**, 2797 (1982).

[51] G. Dresselhaus, M. S. Dresselhaus, and P. C. Eklund, Phys. Rev. B **45**, 6923 (1992).

[52] R. E. Stanton and M. D. Newton, J. Phys. Chem. **92**, 2141 (1988).

[53] F. Negri, G. Orlandi, and F. Zerbetto, Chem. Phys. Lett. **144**, 31 (1988).

[54] A. Warshel and M. Karplus, J. Am. Chem. Soc. **94**, 5612 (1974).

[55] Z. C. Wu, D. A. Jelski, and T. F. George, Chem. Phys. Lett. **137**, 291 (1987).

[56] S. J. Cyvin, E. Brendsdal, B. N. Cyvin, and J. Brunvoll, Chem. Phys. Lett. **143**, 377 (1988).

[57] D. E. Weeks and W. G. Harter, J. Chem. Phys. **90**, 4744 (1989).

[58] R. A. Jishi, R. M. Mirie, and M. S. Dresselhaus, Phys. Rev. B **45**, 13 685 (1992).

[59] D. A. Dixon, B. E. Chase, G. Fitzgerald, and N. Matsuzawa, J. Phys. Chem. **99**, 4486 (1995).

[60] T. Hara, J. Onoe, and K. Takeuchi, Phys. Rev. B **63**, 115412 (2001).

[61] G. Onida, W. Andreoni, J. Kohanoff, and M. Parrinello, Chem. Phys. Lett. **219**, 1 (1994).

[62] P. Pulay and F. Török, J. Mol. Struct. **29**, 1123 (1975); P. Pulay, G. Fogarasi, G. Pongor, J. E. Boggs, and A. Vargha, J. Am. Chem. Soc. **105**, 7037 (1983).